

Meta-PINNs: Meta-Learning Enhanced Physics-Informed Machine Learning Framework for Turbomachinery Flow Predictions under Varying Operation Conditions

Yuling Han, Zhihui Li*, Zhibin Yu

*Department of Mechanical and Aerospace Engineering, School of Engineering,
University of Liverpool, Liverpool, UK*

{yuling.han, zhihui.li, zhibin.yu}@liverpool.ac.uk

ABSTRACT

Coupling physics with machine learning models has shown great potential for solving fluid dynamics problems governed by partial differential equations. However, conventional methods, such as physics-informed neural networks, often suffer from slow convergence, unstable training, and limited generalization across different flow conditions. To overcome these challenges, this study proposes a novel meta-learning enhanced physics-informed neural networks (Meta-PINNs) framework, which integrates a meta-optimization strategy into the training process. The approach allows the model to automatically adapt its learning process to varying physical regimes, thereby substantially improving both training efficiency and predictive robustness. The proposed Meta-PINNs model is evaluated on two representative flow problems: (1) unsteady flow around a circular cylinder at multiple inlet Reynolds numbers, and (2) steady turbulent flow within a compressor cascade passage at various angles of attack. In both cases, the extrapolation performance of the developed framework is comprehensively tested by predicting the flow fields at Reynolds numbers and angles of attack that are not included in the training set. The results demonstrate that Meta-PINNs achieve a 1-2 order-of-magnitude improvement in accuracy over vanilla physics-informed neural networks and standard neural networks, while reducing computational cost by up to 95.7 % and 92.1 %, respectively. It successfully captures the sequential patterns of key flow features such as pressure and velocity distributions under unseen conditions. Thus, the findings confirm that the Meta-PINNs framework offers a notable improvement in convergence and generalization over existing machine learning approaches, providing a promising pathway toward smart simulations of complex turbomachinery flows.

Keywords: Meta-learning; Physics-Informed Neural Networks; Turbomachinery Flow; Various Operation Conditions

1 INTRODUCTION

Cost-efficient prediction of turbomachinery flows in terms of aerodynamic efficiency, pressure ratio and stability margin is central to design optimization of modern gas turbines and aeroengines [1]. Conventional computational fluid dynamic (CFD) tools based on finite volume [2] and finite elements [3] approaches remain the primary way for such analyses. However, the computational cost is prohibitive when high-fidelity flow fields are required for refined turbomachinery designs with geometric variations or when predictions must be generated across a range of operating conditions, particularly during iterative design stages.

Scientific machine learning (SciML) methods have emerged as powerful surrogates for complex physical simulations by leveraging the rapid development of advanced neural networks such as deep neural networks [4], convolutional neural networks [5], graph neural networks [6], Transformer [7], etc. Most of these surrogate models are purely data-driven natures, where large, labeled datasets are required to guide the model to learn the underlying patterns in hidden spaces. However, the data-driven SciML models generally show poor generalization performance outside the training distributions, especially in off-design operating

conditions. As a result, physically inconsistent results are output from these models when extrapolating [8].

To mitigate the generalization issues from data-driven SciML models, a straightforward way is to enforce the governing conservation physics into the training process. Inspired by this, physics-informed neural networks (PINNs) [9] have been proposed by embedding the physical constraints in form of partial differential equations (PDEs) in conjunction with boundary/initial conditions into the loss terms. PINNs demonstrate unique advantages over conventional CFD approaches for solving inverse problems, as they enable the reconstruction of the entire flow field from sparse observational data, which is particularly promising for digital twin applications. More recently, PINNs also have been applied in turbomachinery flow simulations [10-11].

Although some advances achieved in PINNs-based frameworks, several limitations are exposed in practical applications: 1) vanilla PINNs always suffer from convergence issues especially in fluid simulation scenarios due to the gradient pathology; 2) even converged, PINNs are typically tailored to the specifically boundary condition setup, and full retraining is necessary under varying boundary conditions. To address these challenges, meta-learning or “learning to learn” strategy [12] is proposed as a paradigm-shifting approach that enables rapid adaptation of PINNs to new boundary conditions using only a small amount of additional data, i.e., few-shot learning. During a meta-learning phase, the meta-learning based PINNs (Meta-PINNs) learn a set of shared parameters or latent representations that serve as a good initialization for solving various tasks. At meta-test phase, Meta-PINNs rapidly adapts to the previously unseen operating conditions with sparse collation points within a few training iterations. As a result, the physical flow fields can be predicted at a significantly reduced computational cost.

The previous studies demonstrated that Meta-PINNs significantly reduced training time and improved generalization performance when solving a family of PDEs. Cheng and Alkhalifah [13] demonstrated that the convergence speed and prediction accuracy were significantly improved in estimating seismic wavefield when compared to vanilla PINNs. Toloubidokhti et al. [14] further enhanced Meta-PINNs by introducing adaptive loss weights and allocating optimal residual points across different tasks. The superior performance of Meta-PINNs compared to vanilla PINNs was validated through several benchmark tests. Meta-PINNs have also been successfully applied to solve nonlinear Schrodinger equation in previous study [15].

However, the majority of existing Meta-PINNs studies have been limited to canonical PDE benchmarks, leaving a significant gap between methodological research and real-world industrial applications, especially for complex turbomachinery flow simulations. Motivated by these challenges, we proposed a Meta-PINNs-based framework for complex engineering flow simulations under varying conditions. As far as the authors are aware, this is the first attempt to adapt Meta-PINNs for turbomachinery flow simulations.

In this study, the fundamental methodologies of Meta-PINNs are shown in Section 2. The Meta-PINNs-based framework is then developed and benchmarked on two-dimensional (2D) cylinder flow cases with varying inlet Reynolds numbers in Section 3. Subsequently, the benchmarked framework is tailored for turbomachinery application where its performance is evaluated on 2D compressor cascade flows under different incoming attack angles in Section 4. Major conclusions are drawn at the end.

2 NUMERICAL METHODS

The methodologies employed in this work are detailed in this section, together with the formulation of the proposed Meta-PINN framework and its application to two representative flow configurations: the unsteady laminar wake behind a circular cylinder under varying Reynolds numbers, and the steady NACA-65 profile-based linear compressor cascade flow under varying angles of attack. Benchmark assessments and the overall dataset generation procedures are also provided to evaluate the effectiveness of the adopted methods.

2.1 Governing Equations

The flow in both configurations is described by the incompressible Navier–Stokes equations. For the compressor cascade case, the incompressible assumption is justified as the flow corresponds to a low-speed compressor cascade operating at a low Mach number approximately 0.12. Under such conditions, compressibility effects are negligible, and the pressure rise is primarily associated with flow deceleration in accordance with Bernoulli’s principle. In addition, the numerical setup is designed to reproduce the experimental conditions reported in the low-speed compressor cascade experiments conducted at École

Centrale de Lyon, further supporting the validity of the incompressible flow assumption.

The continuity equation is:

$$\nabla \cdot \mathbf{u} = 0 \quad (1)$$

where $\mathbf{u} = (u, v)$ is the velocity.

The general momentum equation is written as:

$$\frac{\partial \mathbf{u}}{\partial t} + \nabla \cdot (\mathbf{u} \otimes \mathbf{u}) = -\nabla p + \nabla \cdot (2\nu_{\text{eff}}\mathbf{S}) \quad (2)$$

where p is static pressure, and ν_{eff} is the effective viscosity. The strain-rate tensor \mathbf{S} is:

$$\mathbf{S} = \frac{1}{2} (\nabla \mathbf{u} + (\nabla \mathbf{u})^T) \quad (3)$$

The two flow cases differ only in how ν_{eff} is defined. For the cylinder wake, the flow is laminar and the effective viscosity can be written as:

$$\nu_{\text{eff}} = \nu \quad (4)$$

where ν represents the molecular viscosity.

For the compressor cascade flow, the flow is turbulent, and the effective viscosity includes the eddy viscosity:

$$\nu_{\text{eff}} = \nu + \nu_t \quad (5)$$

where ν_t represents the turbulent viscosity from one-equation Spalart-Allmaras (SA) [16] model.

2.2 CFD Simulation and Dataset Preparation

Before using the CFD solutions as training data for the Meta-PINNs, a complete numerical simulation module is constructed using *SU2* [17] for each flow configuration. *SU2* is an open-source finite-volume-based CFD solver designed for multiphysics analysis and aerodynamic shape optimization. In this study, a velocity-pressure coupling scheme is used to update the flow velocity and pressure simultaneously at each iteration. For unsteady simulations, second-order dual-time stepping is employed for time marching. The *SU2* simulation stops when the maximum residual drops below 10^{-6} or when the maximum number of iterations is reached. The key design parameters and boundary conditions for each configuration are listed in Tables 1 and 2.

Table 1 Reference values for cylinder flow

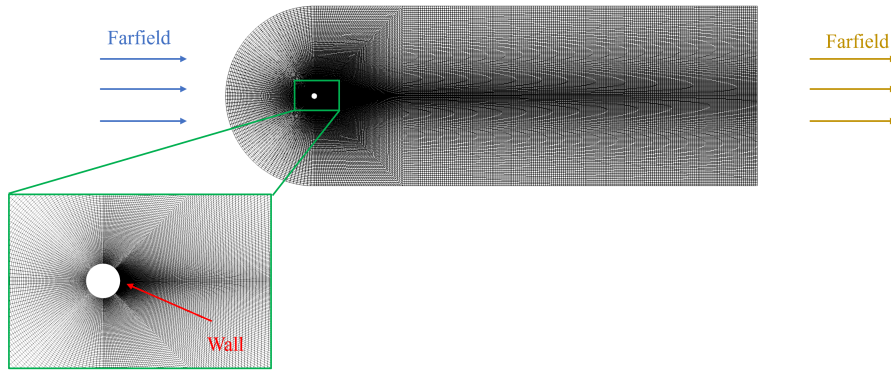
Parameter	Value
Kinematic Viscosity	1.00e-05 $\frac{m^2}{s}$
Density	1 kg/m^3
Inlet Total Pressure	0.02 Pa
Cylinder Diameter	0.01 m
Domain Length	0.3 m
Inlet Velocity Magnitude	[0.2 m/s , 0.25 m/s]

Table 2 Reference values for compressor cascade flow

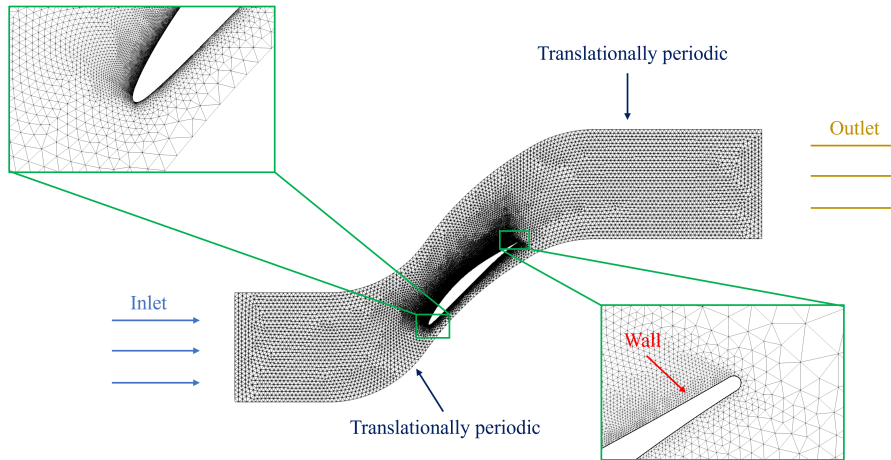
Parameter	Value
Kinematic Viscosity	1.51e-05 $\frac{m^2}{s}$
Density	1.225 kg/m^3
Inlet Total Pressure	980 Pa

Parameter	Value
Inlet Velocity Magnitude	40 m/s
Chord length	0.15 m
Design upstream flow angle	54.31°
Design downstream flow angle	31.09°
Aspect ratio	2.47
Solidity	1.12

For each flow case, the *SU2* solutions and the Meta-PINNs predictions are evaluated on the same computational mesh graph, allowing for a direct pointwise comparison. Fig. 1(a) illustrates the computational domain and mesh topology for the unsteady cylinder flow with a velocity inlet and far-field atmospheric conditions. A no-slip boundary condition is imposed on the cylinder surface. An H-type mesh is employed in the wake region, while an O-type mesh is used upstream of the cylinder. The total number of mesh cells is approximately 70,000. For the compressor cascade case, an unstructured mesh is generated within the passage, with local refinement near the blade surfaces. A matched translational periodic boundary condition is applied on the upper and lower boundaries to account for the influence of adjacent blades. The blade is intentionally shifted toward the lower periodic boundary to provide additional space for the flow separation developing along the suction surface. The total mesh count for this case is approximately 32,000.



(a)



(b)

Fig. 1 (a) Computation domain and mesh topology for circular cylinder flow case (b) Computation domain and mesh topology for compressor cascade flow case

For the cylinder flow case, the numerical simulation is first run for several shedding periods, and snapshots of velocity and pressure are extracted after the cylinder wake flow reaches a periodic pattern. For the compressor cascade, the steady solutions for the velocity, pressure, and effective viscosity fields are obtained. All fields are postprocessed using *Paraview* and serve as the datasets for Meta-PINNs training, validation and testing. The accuracy of the numerical setup is validated by comparing the simulation results with available experimental measurements before using them as training datasets.

Figure 2(a) depicts the distribution of Strouhal number (St) as a function of the inlet Reynolds number Re . Strouhal number is a dimensionless parameter characterizing the vortex-shedding frequency in unsteady flows. It is defined as

$$St = \frac{fD}{U_\infty} \quad (6)$$

where f is the vortex-shedding frequency, D is the characteristic length, and U_∞ is the free stream velocity. The blue crosses represent the simulation results from *SU2* and the orange dots mean the experimental data from Ref. [18]. The Strouhal number generally increases with Reynolds number, indicating that the vortex shedding frequency becomes higher at larger Reynolds numbers. The simulation results well capture this trend.

Figure 2(b) shows the comparison between the simulation results and experimental data [19] for the cascade pressure coefficient (C_p) along the chordwise direction at the condition of the angle of attack $\alpha = 0^\circ$. The pressure coefficient is a nondimensional measure of the pressure relative to the free-stream static pressure, defined as

$$C_p = \frac{p - p_\infty}{\frac{1}{2}\rho U_\infty^2} \quad (7)$$

where p is the local static pressure, p_∞ is the free stream static pressure, ρ is the fluid density, and U_∞ is the free stream velocity. The results demonstrate excellent agreement between the predicted pressure coefficient and the experimental measurements. These strong agreements confirm the correctness of the numerical setup and indicate that the resulting solutions serve as reliable reference datasets for training the machine learning models.

Before being used for training and evaluation, all flow field physical quantities are normalized. Spatial coordinates are normalized by the characteristic length D , velocity by the free-stream velocity U_∞ , pressure by $\frac{1}{2}\rho U_\infty^2$, and effective viscosity ν_{eff} by $U_\infty D$. All flow field results and error metrics reported in this study are based on these normalized variables.

2.3 Physics-Informed Neural Networks

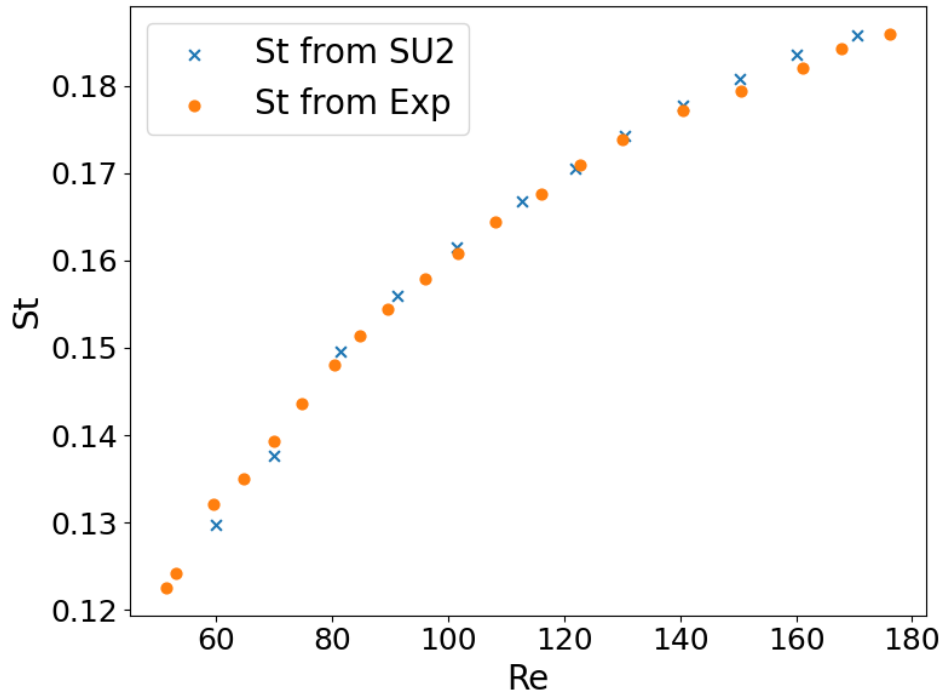
A fully connected neural network is generally employed to approximate the mapping from spatial coordinates in conjunction with operation condition parameters to target flow variables. For the cylinder flow case, the network inputs are (x, y, t, Re) , which represent the Cartesian coordinates, time, and Reynolds number, and the model outputs are (u, v, p) , which represent the velocity components and static pressure. For the compressor cascade case, the inputs are $(x, y, \sin \alpha, \cos \alpha)$, which represent the Cartesian coordinates and the trigonometric encoding of the angle of attack α , and the outputs are $(u, v, p, \nu_{\text{eff}})$, which represent the velocity components, static pressure, and effective turbulent viscosity, respectively.

Automatic differentiation is used to evaluate spatial and temporal derivatives in the PDE residuals. For a set of trainable parameters θ , the physics-informed loss $L_{\text{phys}}(\theta)$ is defined as:

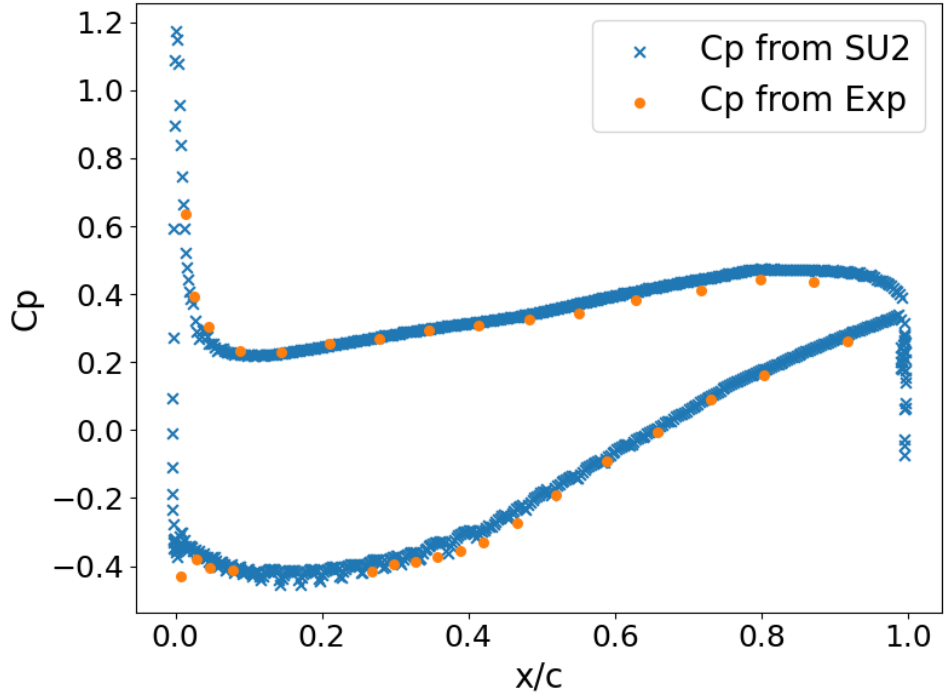
$$L_{\text{phys}}(\theta) = \text{MSE}(\mathcal{R}_{\text{mom}}) + \text{MSE}(\mathcal{R}_{\text{cont}}) \quad (8)$$

where MSE represents the mean squared error, and \mathcal{R}_{mom} and $\mathcal{R}_{\text{cont}}$ denote the residuals of the momentum and continuity equations, respectively. Supervised losses based on available data points $L_{\text{data}}(\theta)$ are incorporated as:

$$L_{\text{data}}(\theta) = \text{MSE}(u_\theta, u) + \text{MSE}(p_\theta, p) + \text{MSE}(\nu_{\text{eff},\theta}, \nu_{\text{eff}}) \quad (9)$$



(a)



(b)

Fig. 2 (a) Strouhal number St comparison between experiment data and CFD results (b) Static pressure coefficient C_p comparison between experiment data and CFD results

where u_θ , p_θ , $\nu_{eff,\theta}$ represents the predicted velocity components, static pressure and effective eddy viscosity, respectively. The overall PINN loss is then given by:

$$L_{PINN}(\theta) = \omega_d L_{data}(\theta) + \omega_p L_{phys}(\theta) \quad (10)$$

where ω_d and ω_p denote the adaptive weighting coefficients for each residual loss term, which are typically annealed during training to stabilize convergence.

2.4 Meta-Learning Framework

To enable fast adaptation of the PINNs to previously unseen operating conditions, a meta-learning strategy is adopted. Each case with a varying Reynolds number or angles of attack defines a task \mathcal{T}_i , consisting of a support set \mathcal{D}_i^{sup} for inner-loop adaptation, and a query set \mathcal{D}_i^{qry} for meta-objective evaluation. Fig. 3 shows the architecture of the meta-learning PINN framework.

During meta-training, the model parameters θ are first adapted to each task after a small number of gradient steps:

$$\theta'_i \leftarrow \theta - lr \nabla_{\theta} L_{PINN}(\theta; \mathcal{D}_i^{sup}) \quad (11)$$

where lr is the inner loop learning rate, θ'_i represent the trained parameters for each case. The meta-objective aggregates the performance of adapted parameters:

$$L_{meta}(\theta) = \sum_i L_{PINN}(\theta'_i; \mathcal{D}_i^{qry}) \quad (12)$$

where $L_{meta}(\theta)$ is the sum of PINNs residual loss for the query set. The outer-loop update follows true meta-training:

$$\theta^* \leftarrow \theta - \beta \nabla_{\theta} L_{meta}(\theta) \quad (13)$$

where β denotes the outer loop learning rate. This two-level optimization yields a general purpose set of initial model parameters θ^* that can quickly adapt to new, unseen Reynolds numbers or angles of attack with few additional data and physics constraints.

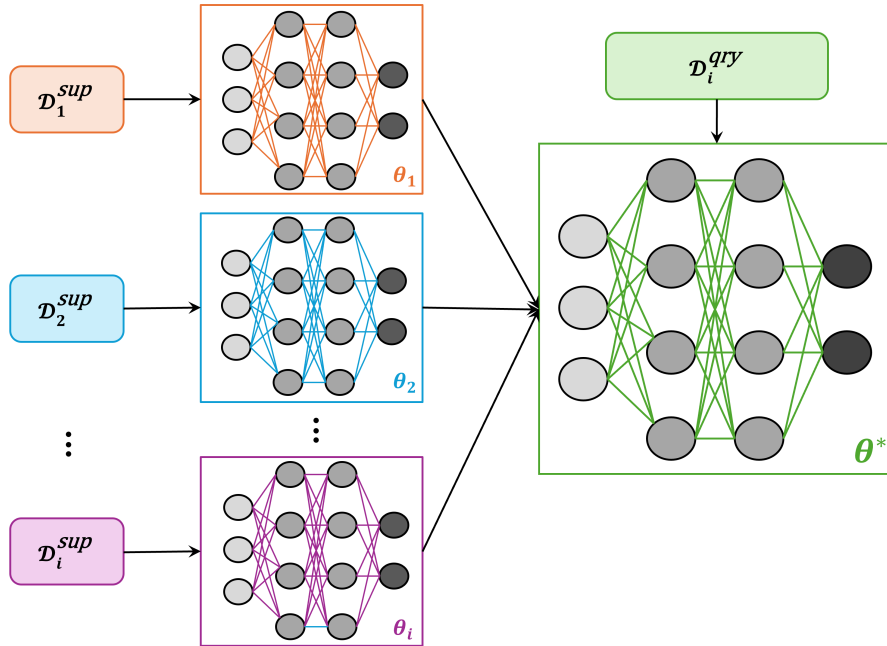


Fig. 3 Architecture of Meta-PINNs framework

2.5 Training Datasets and Task Construction

For cylinder wake, flow-field snapshots at Reynolds numbers $Re = \{200, 210, 220, 230, 240, 250\}$ are generated using *SU2* solvers and serve as training dataset for Meta-PINNs. The dataset contains velocity and pressure fields over 10 uniformly spaced temporal snapshots per shedding cycle, covering 5 fully developed vortex shedding periods, resulting in a total of 50 snapshots. The test tasks correspond to the new conditions with $Re = \{260, 300\}$, representing extrapolative generalization. The training Reynolds numbers are uniformly sampled within a moderate range to capture the main vortex-shedding dynamics, while higher Reynolds numbers are reserved for extrapolation to assess generalization beyond the training regime.

For the compressor cascade, two types of training tasks are constructed to evaluate both interpolation and extrapolation performance. The training angles of attack are $\alpha = \{0^\circ, 1^\circ, 2^\circ, 3^\circ, 4^\circ, 5^\circ\}$. In the interpolation study, the model is tested on the angles of attack of $\alpha = \{0.5^\circ, 1.5^\circ, 2.5^\circ, 3.5^\circ, 4.5^\circ\}$. In the extrapolation study, the training tasks are chosen below the target range, the model is tested on the angles of attack of $\alpha = \{6^\circ, 7^\circ, 8^\circ, 9^\circ, 10^\circ\}$. This setup is designed to evaluate the ability of the model to generalize to higher angles of attack, where flow separation and nonlinear aerodynamic effects become more pronounced. The Meta-PINNs are implemented in the *PyTorch* environment, using 6 hidden layers with 128 neurons in each layer. The trainable parameters in the model are then fine-tuned using the *Adam* optimizer [20].

2.6 Computing Facility

All training and testing procedures in this study were carried out on the high-performance computing (HPC) platform *Barkla* at the University of Liverpool. The training processes of Meta-PINNs, PINNs and NNs were conducted on one *NVIDIA H100* GPU card. All tests were performed using the same node configuration to ensure a fair comparison of computational cost.

3 BENCHMARK TESTS ON CYLINDER FLOW

To evaluate the generalization capability of the proposed Meta-PINNs framework across different flow regimes, the unsteady laminar wake behind a circular cylinder is first investigated. The Meta-PINNs are trained using flow-field data corresponding to Reynolds numbers from 200 to 250. These cases represent moderate laminar vortex shedding conditions with similar global structures but subtle variations in shedding frequency and wake width. Figs. 4 and 5 present a comparison between the Meta-PINNs predictions and the *SU2* ground-truth results for the velocity components and pressure contours at two new Reynolds numbers, 260 and 300.

It can be observed that for Reynolds numbers of 260 and 300, the Meta-PINNs accurately predict the unsteady velocity and pressure fields at various sampling instants throughout a complete vortex shedding cycle T . The overall wake structure remains well preserved, and the predicted velocity and pressure fields are highly consistent with the CFD results across most regions. In the downstream area, the alternating Kármán vortex street is clearly captured, and the relative locations and strengths of the predicted vortex cores closely match those in the ground-truth flow fields. These results demonstrate that Meta-PINNs effectively learns the temporal evolution of the vortex street and provides accurate flow field predictions throughout the entire vortex shedding cycle.

The error distributions shown in Figs. 4 and 5 further highlight the predictive characteristics of Meta-PINNs. In most regions of the flow field, the pointwise relative errors remain small, consistent with the overall agreement observed between the predicted and ground-truth velocity and pressure fields. The largest errors are mainly concentrated downstream the circular cylinder, where the velocity gradients are high and the local flow structures vary rapidly. In these regions, slight deviations in the predicted vortex position or strength can lead to locally amplified errors. Despite these localized discrepancies, the primary wake features are accurately captured. This further confirms that Meta-PINNs are capable of learning the dominant wake dynamics, with only minor differences appearing in the most unstable regions.

The relative error fields also clearly reveal the distinct error patterns at different Reynolds numbers. In the $Re = 260$ test case, the prediction errors of both the velocity and pressure are noticeably smaller than those for case with $Re = 300$. This is because the case at $Re = 260$ lies closer to the Reynolds number range used for training, and its wake dynamics more closely resemble the flow characteristics present in the training samples. Since the Reynolds number of 300 lies well outside the training range, the Meta-PINNs performs a larger step extrapolation, resulting in increased errors in certain regions, particularly within

the highly unstable vortex cores. Nevertheless, the primary wake structures are still successfully captured.

To further quantify the prediction accuracy beyond the visualized results, the root-mean-square error (RMSE) of the velocity and pressure fields for the different test Reynolds numbers are compared. The RMSE analysis enables a more detailed assessment of the model performance and reveals how the prediction error varies as the flow complexity increases. By comparing the results at Re of 260 and 300, the influence of the test Re on the generalization capability of Meta-PINNs becomes more clearly evident.

As shown in Tab. 3, both the velocity and pressure fields exhibit relatively small RMSE values at $Re = 260$, indicating a low level of overall prediction error. In contrast, all predicted physical quantities show a clear increase in RMSE at $Re = 300$. This increase in error at $Re = 300$ is consistent with the qualitative comparison shown in Figs. 4 and 5. Since extrapolation is inherently more prone to error, the RMSE levels are significantly higher than those at $Re = 260$. To validate the effectiveness of the proposed method, Meta-PINNs performance is compared to the conventional neural networks (NNs) and the standard PINNs in terms of computational cost and prediction accuracy. To ensure a fair comparison, the Meta-PINNs, PINNs, and NNs all employ the same neural network architecture, consisting of six hidden layers with 128 neurons per layer and identical activation functions, such that performance differences are solely attributed to the learning strategy.

Table 3 RMSE comparison of Meta-PINNs predictions at Reynolds numbers 260 and 300 based on normalized flow-field variables

Re	260	300
RMSE_ u	0.004	0.014
RMSE_ v	0.006	0.022
RMSE_ V_m	0.007	0.027
RMSE_ p	0.001	0.002

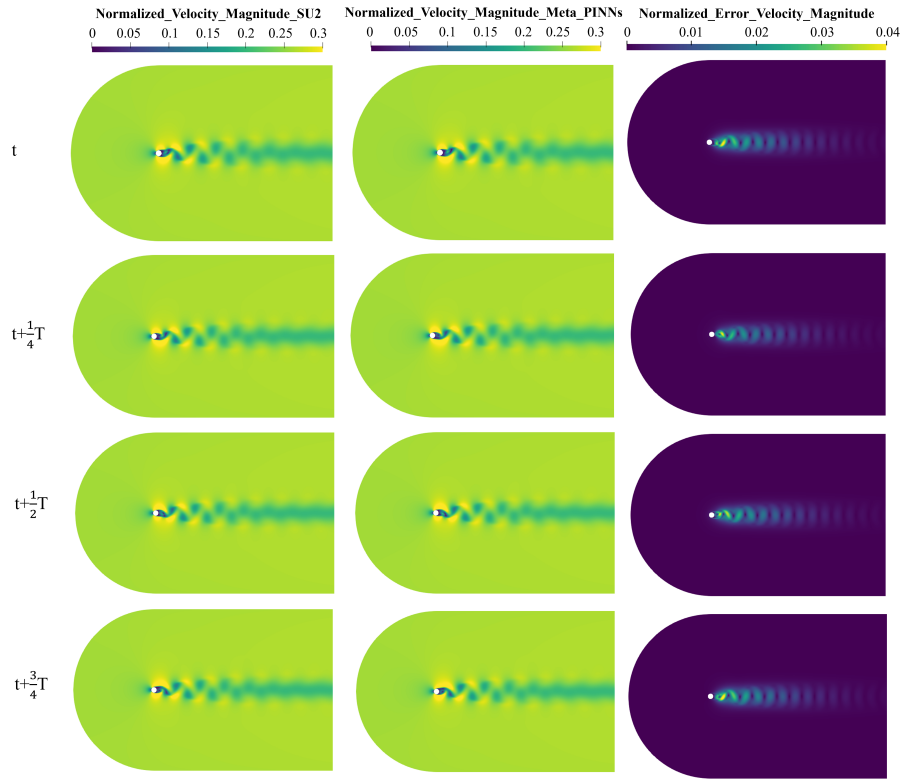
The Strouhal numbers predicted in the Reynolds number range of 200 to 300 are compared with those obtained from CFD simulations, as shown in Fig. 6. Within this range, the Strouhal number increases gradually with Reynolds number, and the Meta-PINNs successfully capture this trend. When the Reynolds number is close to the training data regime, the predicted values align closely with the *SU2* reference results, exhibiting only small errors. As the Reynolds number increases further, Meta-PINNs begin to underestimate the shedding frequency, and the deviation grows, reaching a maximum error smaller than 3.5% at $Re = 300$. The increasing error with Reynolds number can be attributed to the stronger Kármán vortex shedding and the heightened sensitivity of wake dynamics at higher Re . Even so, the predicted Strouhal numbers still correctly characterize the overall trend across the entire test interval.

Table 4 Computational cost and prediction accuracy comparison of Meta-PINNs, PINNs and NNs at $Re = 260$ based on normalized flow-field variables

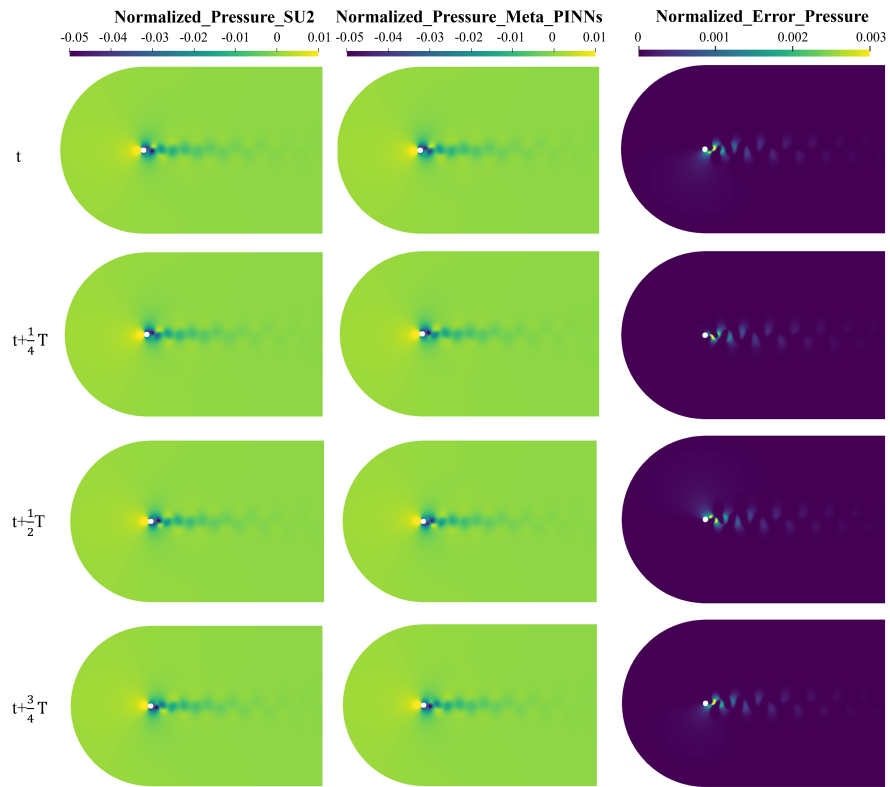
Re	Meta-PINNs	PINNs	NNs
RMSE_ u	0.004	0.244	0.321
RMSE_ v	0.006	0.373	0.533
RMSE_ V_m	0.007	0.255	0.327
RMSE_ p	0.001	0.034	0.438
Time cost	7:59:33	7d-18:43:20	4d-5:24:09

In Table 4, the PINNs are implemented as standard physics-informed neural networks by enforcing the governing equations and boundary conditions through physics-based loss terms, while the NNs serve as purely data-driven baselines without physical constraints. The prediction accuracy is evaluated using RMSE computed on normalized velocity and pressure fields. The computational cost reported corresponds to the total wall-clock time required for model training and prediction.

To validate the effectiveness of the proposed method, Meta-PINNs performance is compared to the conventional neural networks (NNs) and the standard PINNs in terms of computational cost and prediction accuracy. To ensure a fair comparison, the neural architectures in the Meta-PINNs, PINNs, and NNs are



(a)



(b)

Fig. 4 Comparison of the normalized velocity magnitude and pressure fields between CFD and Meta-PINNs at different instants within one shedding cycle for Reynolds number 260

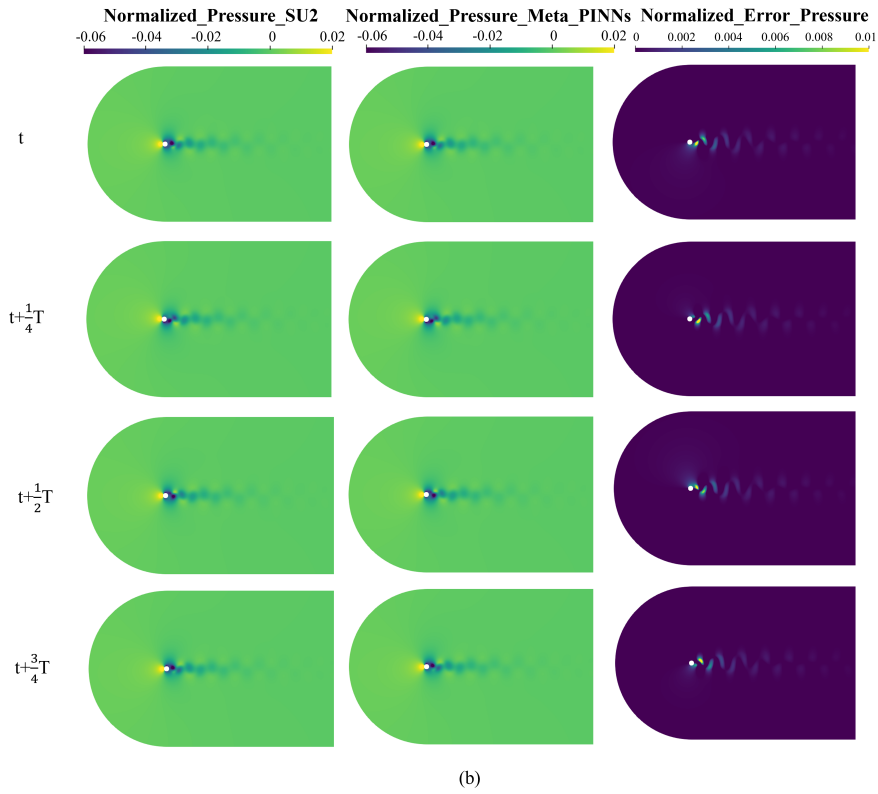
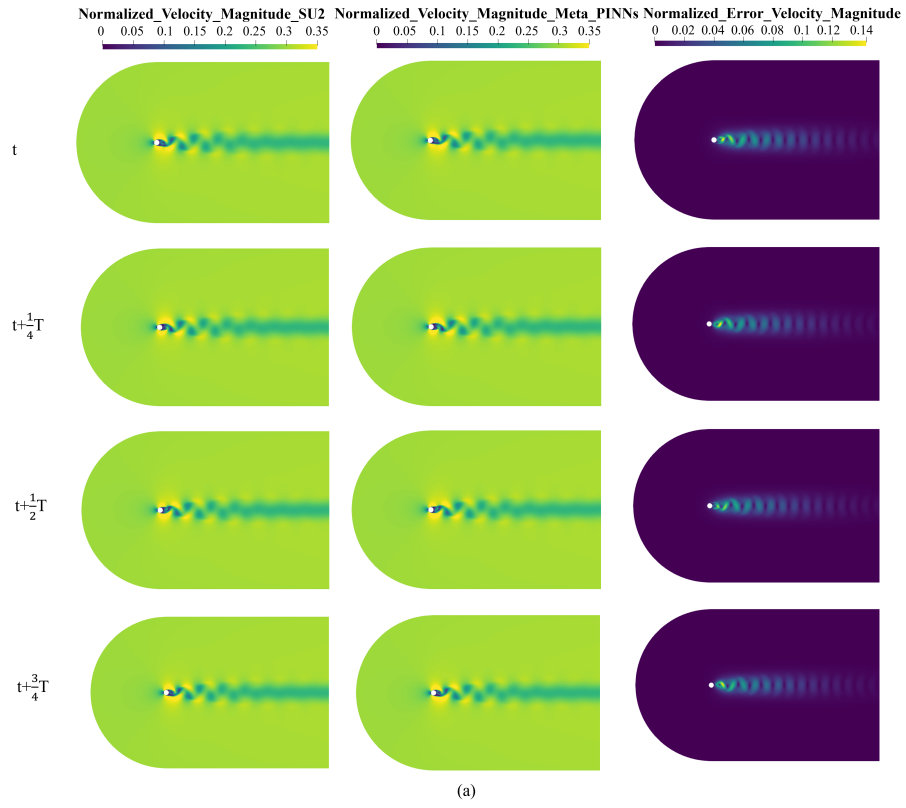


Fig. 5 Comparison of the normalized velocity magnitude and pressure fields between CFD and Meta-PINNs at different instants within one shedding cycle for Reynolds number 300

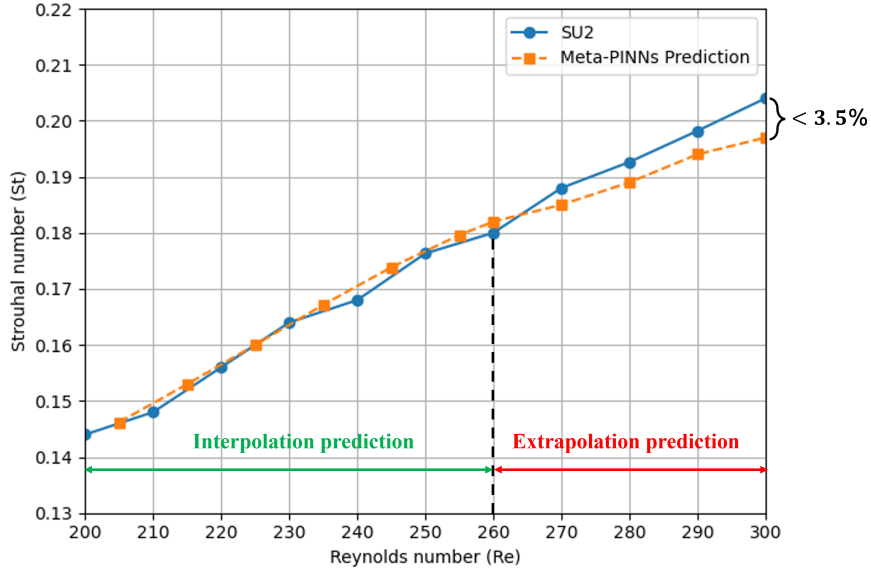


Fig. 6 Strouhal number comparison between CFD results and predictions from Meta-PINNs

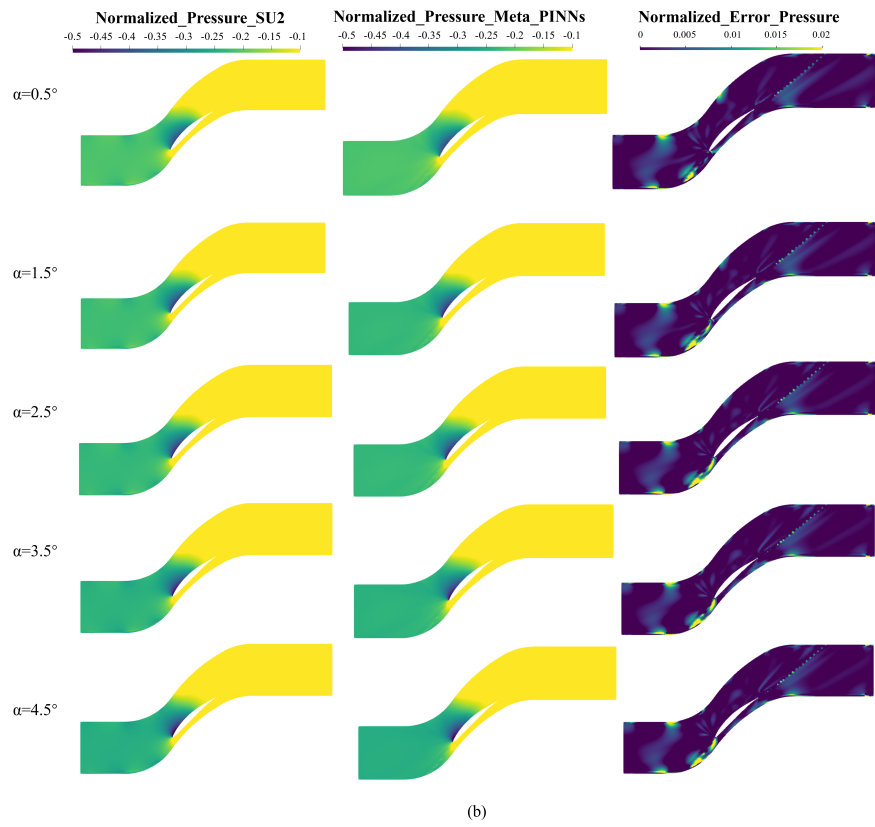
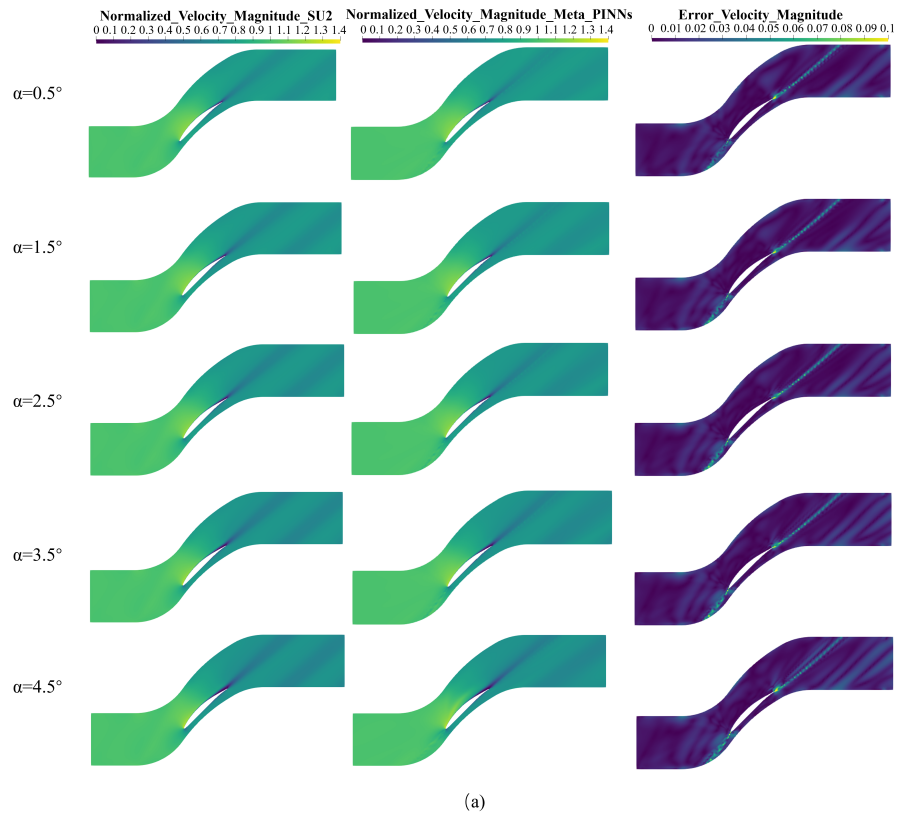
maintained consistently throughout this study. As shown in Table 4, Meta-PINNs outperform both PINNs and NNs in terms of prediction accuracy and training efficiency. In detail, based on the RMSE results, the prediction accuracy of the Meta-PINNs improves by at least 1 to 2 orders of magnitude compared with the PINNs and NNs. Meanwhile, the computational cost is reduced by approximately 95.7 % and 92.1 % relative to the PINNs and NNs, respectively. These results demonstrate that the Meta-PINNs are both more accurate and more efficient for multi-condition flow prediction.

The improved performance of Meta-PINNs over standard PINNs can be attributed to the meta-learning strategy. By learning shared representations across multiple flow conditions during the meta-training phase, Meta-PINNs provide a favorable initialization for new tasks. Consequently, the subsequent training becomes more task-adaptive and converges more efficiently than PINNs trained from scratch, leading to both higher accuracy and lower computational cost.

4 APPLICATION ON COMPRESSOR FLOW

The compressor cascade case uses training data from angles of attack between 0° and 5° . The Meta-PINNs first predict the flow fields at the intermediate angles of attack of 0.5° , 1.5° , 2.5° , 3.5° and 4.5° . Fig. 7(a) shows the velocity vector comparison from $\alpha = 0.5^\circ$ to $\alpha = 4.5^\circ$, including the *SU2* reference fields, the Meta-PINNs predictions and the corresponding errors. The predicted flow field matches the reference solution well across the entire computational domain. The local acceleration in the front region of the suction side is accurately reproduced. The flow direction and streamline curvature within the passage remain consistent with the ground-truth field, and the wake downstream of the trailing edge exhibits the correct strength and thickness. The prediction error remains small across most of the domain. Relatively large local errors are mainly observed in the regions near the inlet and outlet, where the flow is strongly influenced by boundary conditions and undergoes rapid global acceleration or deceleration. These errors primarily originate from boundary-condition-induced global velocity gradients. Although the errors in these regions are larger than those in other parts of the domain, they remain confined to limited areas and do not affect the overall flow structure. This indicates that the Meta-PINNs are able to preserve the dominant topological features of the flow field within the interpolation range and achieve accurate full-field velocity predictions.

From Fig. 7(b), it can be seen that Meta-PINNs also provides accurate predictions of the pressure field, with the overall pressure distribution closely matching the reference results. The low pressure region on the suction side is correctly captured, and the magnitude of the pressure rise on the pressure side is also accurately predicted. The pattern of the pressure distribution within the channel, as well as the direction of the pressure gradients, is consistent with the ground-truth solution. The pressure prediction error



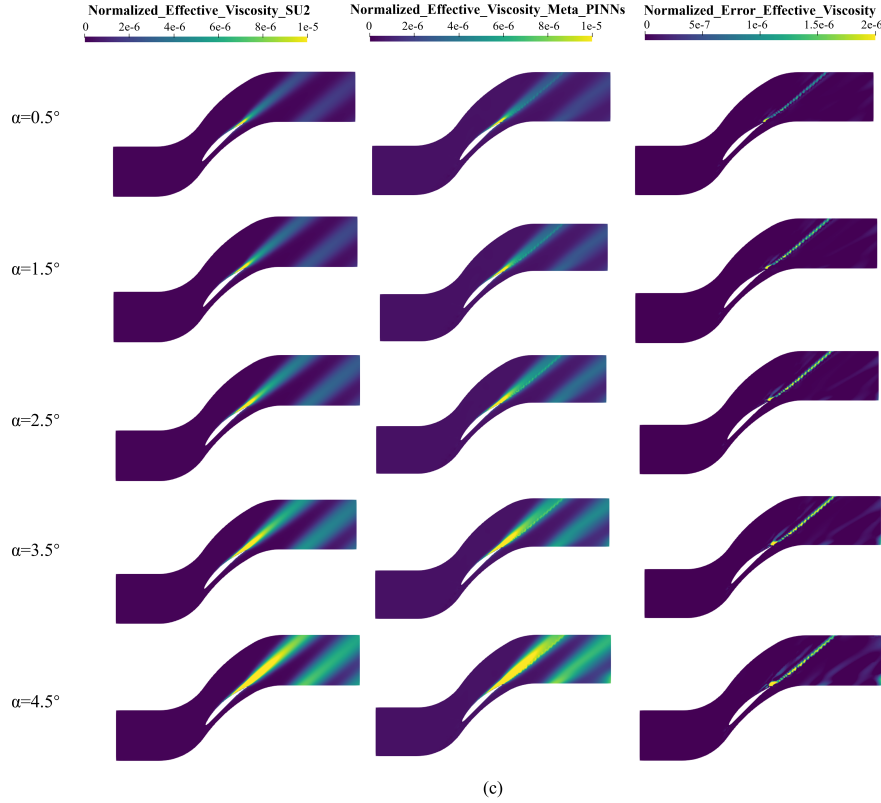
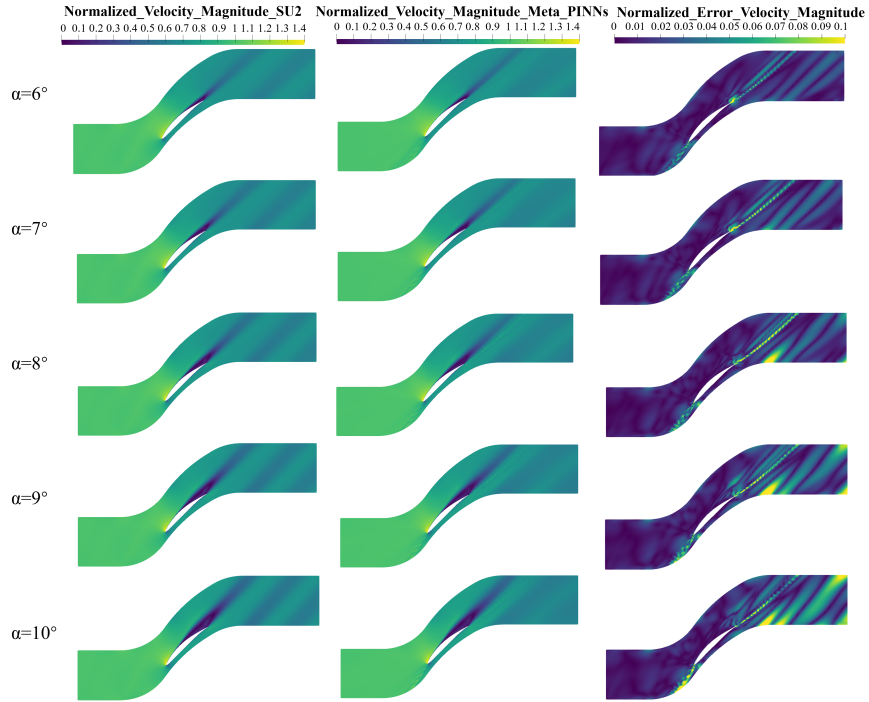


Fig. 7 Comparison of normalized velocity magnitude, pressure, and effective viscosity fields predicted by CFD and Meta-PINNs for angles of attack from 0.5° to 4.5°

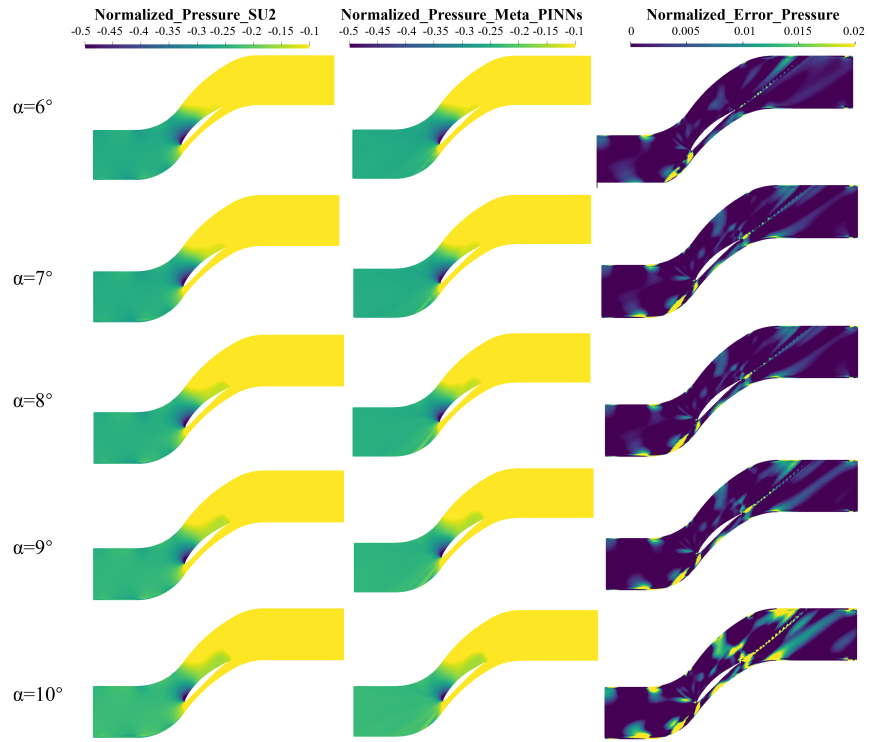
remains small over most of the computational domain, with relatively larger errors primarily concentrated near the inlet and outlet regions, as well as in localized zones where the flow undergoes rapid deformation. These regions are characterized by strong pressure gradients induced by boundary conditions and flow acceleration or deceleration, which makes the pressure field more sensitive to minor prediction deviations. Although the local errors in these areas are comparatively higher, they are confined to limited regions and do not distort the overall pressure distribution. This demonstrates that, under interpolation conditions, Meta-PINNs are capable of accurately capturing the global pressure field while preserving its dominant structural characteristics.

Fig. 7(c) presents a comparison of the effective viscosity fields in the blade cascade case, including the SU2 reference solution, the Meta-PINNs prediction, and the corresponding error distribution. The effective viscosity accounts for both molecular viscosity and turbulent eddy viscosity effects, and is highly sensitive to the generation and transport of turbulence. Overall, the effective viscosity predicted by the Meta-PINNs shows good agreement with the SU2 reference solution within the blade passage. The streamwise distributions and magnitude levels of effective viscosity along both the suction and pressure surfaces are accurately reconstructed, indicating that the model is capable of effectively learning the turbulence intensity characteristics inside the cascade channel. The prediction error of effective viscosity remains small over most of the computational domain and is mainly concentrated in the downstream wake region behind the trailing edge, where a distinct high error band can be observed. In this region, the effective viscosity varies rapidly in space, making the prediction more sensitive to local deviations. Despite the localized increase in error, the discrepancies remain confined to the wake region and do not disrupt the overall structure of the effective viscosity field. This demonstrates that, under interpolation conditions, the Meta-PINNs can reliably reconstruct the effective viscosity distribution.

In the extrapolation tests, the prediction range of Meta-PINNs extends to the angles of attack between 6° and 10° , as shown in Fig. 8. The prediction results show that Meta-PINNs are still able to reconstruct the overall flow structure with reasonable accuracy. The acceleration region on the suction side and the



(a)



(b)

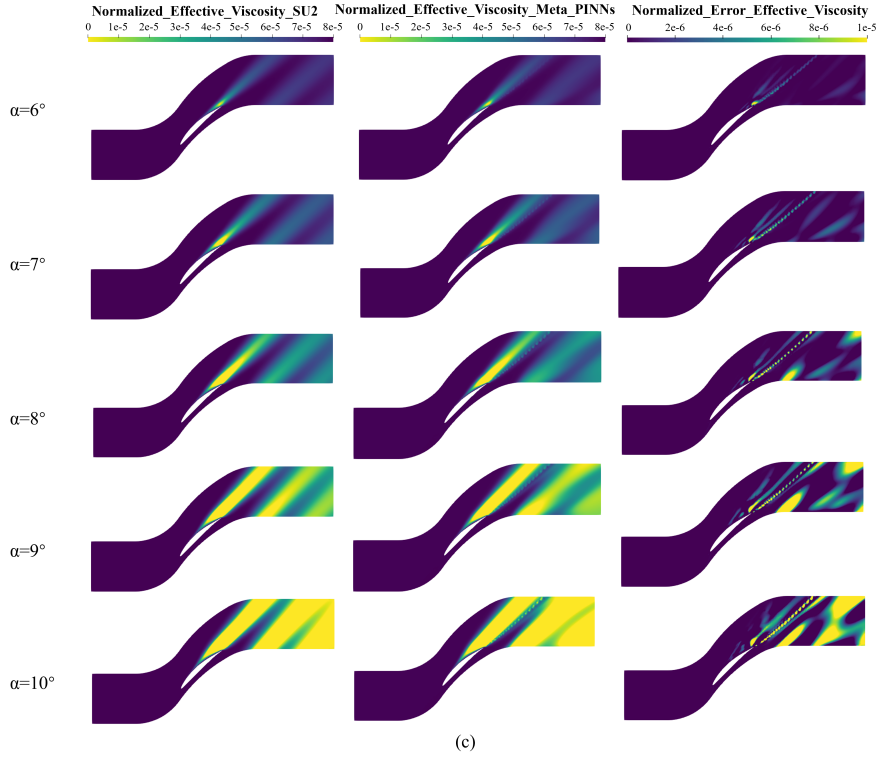


Fig. 8 Comparison of normalized velocity magnitude, pressure, and effective viscosity fields predicted by CFD and Meta-PINNs for angles of attack from 6° to 10°

flow-direction variations inside the channel follow the correct trends, and the wake pattern downstream of the trailing edge remains largely consistent with the reference solution.

Figure 8(a) presents the predicted velocity fields and the corresponding error distributions under extrapolation conditions with angles of attack ranging from 6° to 10° . Overall, the velocity fields predicted by the Meta-PINNs show good agreement with the SU2 reference solutions, and the dominant flow structures are consistently preserved across all operating conditions. Within the blade passage, including both the suction and pressure side regions, the prediction errors remain relatively small, indicating that the primary flow features learned from the training data can be effectively generalized beyond the interpolation range. More noticeable discrepancies are mainly observed near the inlet and outlet regions, where the flow is strongly influenced by boundary conditions and global flow adjustment processes. As the angle of attack further increases, the error distribution downstream of the trailing edge gradually exhibits more distinct structural patterns, with errors predominantly concentrated in the wake region. These discrepancies remain spatially localized and do not significantly affect the overall velocity distribution or the global flow topology. This suggests that the Meta-PINNs retain a robust capability for full-field velocity prediction even under extrapolation conditions.

Figure 8(b) illustrates the pressure error distributions under extrapolation conditions with angles of attack ranging from 6° to 10° . Overall, the pressure fields predicted by the Meta-PINNs show good agreement with the SU2 reference solutions, and the global pressure distribution within the blade passage is consistently preserved across all operating conditions. For all extrapolation cases, relatively larger pressure errors are observed near the inlet and outlet regions. This behavior is expected, as the pressure field is a globally coupled quantity that is strongly constrained by boundary conditions and influenced by the overall flow adjustment process. Consequently, small prediction deviations tend to be amplified near the domain boundaries. In addition to the inlet and outlet regions, another error feature becomes increasingly pronounced with increasing angle of attack: band-shaped error patterns emerge and intensify near the lateral boundaries of the passage. These regions are strongly affected by the periodic boundary matching of the blade cascade, and their sensitivity to changes in operating conditions increases under high-angle-of-attack scenarios. Despite the localized growth of errors with increasing angle of attack,

the dominant pressure topology and the overall loading trends within the passage remain well preserved. This indicates that the Meta-PINNs maintain robust pressure field prediction capability even under extrapolation conditions.

Fig. 8(c) presents the error distributions of the effective viscosity under extrapolation conditions with angles of attack ranging from 6° to 10° . Overall, the effective viscosity predicted by the Meta-PINNs remains in good agreement with the SU2 reference solutions, and the main distribution characteristics inside the blade passage are consistently preserved. Across all extrapolation cases, the prediction error remains small over most of the computational domain. Relatively larger errors are primarily observed near the outlet and in the wake region downstream of the trailing edge. As the angle of attack increases, the error magnitude in these regions gradually increases, while the error distribution remains spatially localized. The increased errors near the outlet and in the wake are associated with strong turbulence production and rapid spatial variations of effective viscosity in these regions, which makes the prediction more sensitive under extrapolation conditions. Despite the localized error amplification at higher angles of attack, the overall structure of the effective viscosity field remains intact, indicating that the Meta-PINNs can reliably reconstruct effective viscosity distributions even beyond the training range.

Table 5 RMSE comparison of Meta-PINNs predictions at different angles of attack, RMSE values are computed based on normalized flow-field variables

α	RMSE_ V_m	RMSE_ p	RMSE_ ν_{eff}
0.5	0.025	0.005	1e-6
1.5	0.025	0.005	1.2e-6
2.5	0.024	0.005	1.5e-6
3.5	0.024	0.006	1.8e-6
4.5	0.025	0.006	2.7e-6
6	0.027	0.007	5e-6
7	0.029	0.008	7.9e-6
8	0.031	0.009	1.3e-5
9	0.032	0.009	1.9e-5
10	0.033	0.009	2.8e-5

Table 5 shows that the quantitative RMSE results are consistent with the trends observed in the flow field visualizations. Under interpolation conditions, corresponding to angles of attack within the training range, the RMSE values of the velocity magnitude V_m , and the pressure p remain close to each other and exhibit only minor variations with respect to the angle of attack. This indicates that when the target conditions lie within the training distribution, the Meta-PINNs maintain stable and consistent prediction accuracy across different flow variables.

Under extrapolation conditions, the RMSE values increase monotonically as the angle of attack rises from 6° to 10° . The growth of errors reflects the increasing difficulty of prediction as the operating condition moves further away from the training range. While the RMSE values of the velocity components and pressure increase gradually, the effective viscosity exhibits a more pronounced rise in error magnitude, indicating a higher sensitivity to extrapolation. This behavior is consistent with the fact that the effective viscosity is closely related to turbulence production and transport processes, which become more complex at higher angles of attack.

Overall, despite the gradual increase in error levels under extrapolation conditions, the magnitude of the RMSE remains controlled for all variables, demonstrating that the Meta-PINNs retain robust predictive capability even when applied to flow conditions beyond the training range.

Figure 9 shows the distribution of total pressure loss coefficient ξ with respect to the angle of attack. The total pressure loss coefficient characterizes the aerodynamic loss within the compressor cascade by quantifying the decrease in total pressure as the flow traverses the passage. It is defined as:

$$\xi = \frac{p_{t,\infty} - p_{t,out}}{\frac{1}{2}\rho U_\infty^2} \quad (14)$$

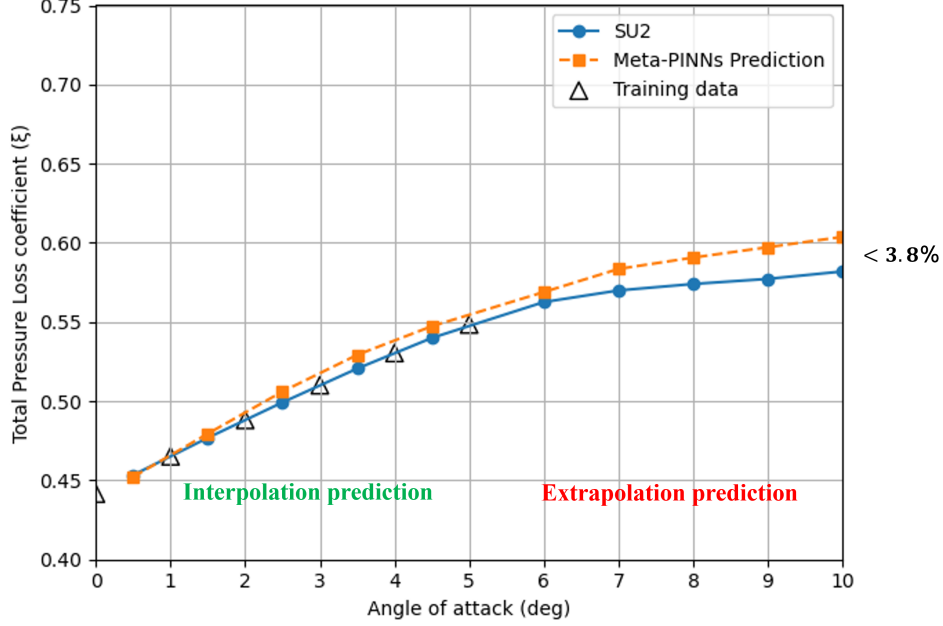


Fig. 9 Total pressure loss coefficient comparison between CFD results and prediction from Meta-PINNs

where $p_{t,\infty}$ is the inlet total pressure, $p_{t,out}$ is the total pressure at the outlet surface, U_∞ is the inlet free-stream velocity. A higher value of ξ indicates a greater aerodynamic loss in the flow passage. The results show that within the interpolation angle-of-attack range of 0.5° to 5° , the total pressure loss coefficients predicted by Meta-PINNs closely match the SU2 results. Both the trend of increasing loss with angle of attack and the corresponding magnitude are accurately captured, indicating that the Meta-PINNs can reliably learn the dominant loss mechanisms when the operating condition remains close to the training range.

In the extrapolation regime, the Meta-PINNs continue to provide reliable predictions at moderate angles of attack, particularly at 6° and 7° , where the predicted loss coefficients remain close to the reference results. As the angle of attack increases further, the deviation between the predicted and reference values gradually becomes more pronounced. Although the Meta-PINNs exhibit a tendency to slightly overestimate the growth rate of total pressure loss at higher angles of attack, they are still able to follow the overall nonlinear evolution of the loss with respect to the angle of attack. Overall, despite a reduction in quantitative accuracy under high-angle-of-attack extrapolation conditions, the prediction error of the total pressure loss coefficient remains bounded within 3.8%, demonstrating that the Meta-PINNs retain a robust predictive capability even beyond the training range.

Table 6 computational cost and prediction accuracy comparison of Meta-PINNs, PINNs and NNs of $\alpha = 10^\circ$ based on normalized flow-field variables

Re	Meta-PINNs	PINNs	NNs
RMSE_ u	0.022	0.154	0.206
RMSE_ v	0.024	0.143	0.172
RMSE_ V_m	0.033	0.197	0.24
RMSE_ p	0.009	0.106	0.122
Time cost	8:58:06	28:41:25	10:03:47

As shown in Tab. 6, Meta-PINNs achieve the best prediction accuracy among the three models for the flow prediction at $\alpha = 10^\circ$. The traditional PINNs perform better than the NNs but still fall noticeably short of Meta-PINNs. Since the NN does not incorporate any physical constraints, it exhibits the largest errors. A similar trend is observed in terms of computational cost. Meta-PINNs require only a small number of adaptive updates for each new angle of attack, resulting in the shortest runtime of per task.

In contrast, the PINNs must be trained from scratch for every operating condition, making it the most time-consuming method. The NNs are faster than the PINNs, but because it still requires retraining for each angle of attack, its overall efficiency remains lower than that of Meta-PINNs. The results demonstrate the Meta-PINNs reduce the computational cost by approximately 45.6% and 10.8% relative to the PINNs and NNs, respectively.

5 CONCLUSIONS

This study proposes a novel Meta-PINNs-based flow-field prediction framework designed to address flow predictions under varying operating conditions. The framework integrates physical constraints with a meta-learning strategy, overcoming the inherent limitations of conventional PINNs. Two representative flow configurations are investigated: unsteady circular cylinder flow with varying Reynolds numbers, and compressor cascade flows under different angles of attack, covering both laminar and turbulent regimes. The main conclusions can be drawn:

- 1) For the cylinder flow case, Meta-PINNs accurately reproduce the Kármán vortex-shedding cycle, wake dynamics, and pressure distribution, achieving the highest prediction accuracy at the lowest computational cost compared with vanilla PINNs and standard NNs. In terms of prediction error, Meta-PINNs improve the prediction accuracy by 1-2 orders of magnitude relative to PINNs and NNs. Meanwhile, the accompanying computational cost is reduced by approximately 95.7 % and 92.1 % compared with PINNs and NNs, respectively.
- 2) For the compressor cascade flow, Meta-PINNs successfully predict velocity vectors, surface pressure distributions, effective viscosity fields and downstream wake structures across a broad range of angle of attack. The total pressure loss coefficient agrees well with the reference data at small and moderate angles of attack. Although deviations occur at a higher angle of attack, with a maximum prediction error of less than 3.8 %, Meta-PINNs still reproduce the correct overall nonlinear increasing trend. Meta-PINNs are still superior to PINNs and NNs in terms of prediction accuracy and computing cost. The results demonstrate the Meta-PINNs reduce the computational cost by approximately 45.6 % and 10.8 % relative to the PINNs and NNs, respectively.
- 3) The meta-learned parameter initialization strategy enables rapid adaptation to new operating conditions. Thus, Meta-PINNs achieve high prediction accuracy for interpolation tasks and maintain reasonable accuracy even for extrapolation cases involving substantial parametric variations. These findings demonstrate the potential of meta-learning to enhance the efficiency and transferability of physics-informed models, making the approach well suited for real-world engineering applications that require fast, cross-condition flow predictions.

Overall, the Meta-PINNs framework exhibits strong adaptability and generalization capability for aerodynamic problems with significant parametric variations. The findings illustrate the potential of meta-learning to enhance the efficiency and transferability of physics-informed models, making it well suited for engineering applications requiring fast, cross-condition flow predictions. Although the present study focuses on two-dimensional benchmark cases, it represents an important first step toward more realistic turbomachinery applications. Future work will extend the proposed Meta-PINNs framework to three-dimensional flow configurations and more complex industrial scale problems.

Conflict of Interest

There are no conflicts of interest

Data Availability Statement

The datasets generated and supporting the findings of this article are obtainable from the corresponding author upon reasonable request.

NOMENCLATURE

\mathbf{u}	Velocity Vector
u	Axial Velocity Component
v	Vertical Velocity Component
V_m	Velocity Magnitude
p	Static Pressure

\mathbf{S}	Strain-Rate Tensor
ν	Molecular Viscosity
ν_{eff}	Effective Viscosity
ν_t	Turbulent Viscosity
S_t	Strouhal Number
f	Vortex-Shedding Frequency
D	Characteristic Length
U_∞	Free-Stream Velocity
C_p	Pressure Coefficients
p_t	Total Pressure
$p_{t,out}$	Outlet Total Pressure
$p_{t,\infty}$	Inlet Total Pressure
p_∞	Free-Stream Static Pressure
ρ	Fluid Density
x	Axial Coordinates
y	Vertical Coordinates
t	Time
Re	Reynolds Number
α	Angle of Attack
θ	Trainable Parameters
θ^*	Initial Model Parameters
$L_{phys}(\theta)$	Physics-Informed Loss
$L_{data}(\theta)$	Data Loss
$L_{meta}(\theta)$	Meta-PINNs' Residual Loss
L_{PINN}	Total Training Loss
\mathcal{R}_{mom}	Residuals of Momentum Equations
\mathcal{R}_{cont}	Residuals of Continuity Equations
ω_d, ω_p	Adaptive Weighting Coefficients
\mathcal{T}_i	Prediction Task
\mathcal{D}_i^{sup}	Support Set
\mathcal{D}_i^{qry}	Query Set
lr	Inner Loop Learning Rate
θ'_i	Trained Parameters for Each Case
β	Outer Loop Learning Rate
T	Full Vortex-Shedding Cycle
ξ	Total Pressure Loss Coefficient
CFD	Computational Fluid Dynamic
Meta-	Meta-Learning Enhanced
PINNs	Physics-Informed Neural Networks
NNS	Neural Networks
PDEs	Partial Differential Equations
PINNs	Physics-Informed Neural Networks
SciML	Scientific Machine Learning

REFERENCES

1. Li, Z. and Zheng, X., 2017. Review of design optimization methods for turbomachinery aerodynamics. *Progress in Aerospace Sciences*, 93, pp.1-23.
2. Moukalled, F., Mangani, L. and Darwish, M., 2016. *The finite volume method in computational fluid dynamics*. Springer.
3. Löhner, R., 2008. *Applied computational fluid dynamics techniques: an introduction based on finite element methods*. John Wiley & Sons.
4. Li, Z., Montomoli, F., Casari, N. and Pinelli, M., 2023. High-dimensional uncertainty quantification of high-pressure turbine vane based on multifidelity deep neural networks. *Journal of Turbomachinery*, 145(11), p.111009.

5. Fukami, K., Fukagata, K. and Taira, K., 2019. Super-resolution reconstruction of turbulent flows with machine learning. *Journal of Fluid Mechanics*, 870, pp.106-120.
6. Li, Z. and Montomoli, F., 2025. Physics-Guided Graph Neural Networks: Numerical Investigation of High-Pressure Turbine Flow. *Journal of Turbomachinery*, 147(12), p.121005.
7. Wu, H., Luo, H., Wang, H., Wang, J. and Long, M., 2024. Transolver: A fast transformer solver for PDEs on general geometries. *arXiv preprint arXiv:2402.02366*.
8. Lino, M., Fotiadis, S., Bharath, A.A. and Cantwell, C.D., 2023. Current and emerging deep-learning methods for the simulation of fluid dynamics. *Proceedings of the Royal Society A*, 479(2275), p.20230058.
9. Cai, S., Mao, Z., Wang, Z., Yin, M. and Karniadakis, G.E., 2021. Physics-informed neural networks (PINNs) for fluid mechanics: A review. *Acta Mechanica Sinica*, 37(12), pp.1727-1738.
10. Li, Z., Montomoli, F. and Sharma, S., 2024. Investigation of compressor cascade flow using physics-informed neural networks with adaptive learning strategy. *AIAA Journal*, 62(4), pp.1400-1410.
11. Hanrahan, S.K., Kozul, M. and Sandberg, R.D., 2025. Data Assimilation of Transitional and Separated Turbomachinery Flows with Physics-Informed Neural Networks. *Journal of Turbomachinery*, 147(11), p.111011.
12. Zhong, L., Wu, B. and Wang, Y., 2023. Accelerating physics-informed neural network based 1D arc simulation by meta learning. *Journal of Physics D: Applied Physics*, 56(7), p.074006.
13. Cheng, S. and Alkhalifah, T., 2024. Meta-PINN: Meta learning for improved neural network wavefield solutions. *arXiv preprint arXiv:2401.11502*.
14. Toloubidokhti, M., Ye, Y., Missel, R., Jiang, X., Kumar, N., Shrestha, R. and Wang, L., 2023. Dats: Difficulty-aware task sampler for meta-learning physics-informed neural networks. In *The Twelfth International Conference on Learning Representations*.
15. Wong, J.C., Ooi, C.C., Gupta, A. and Ong, Y.S., 2022. Learning in sinusoidal spaces with physics-informed neural networks. *IEEE Transactions on Artificial Intelligence*, 5(3), pp.985-1000.
16. Spalart, P. and Allmaras, S., 1992, January. A one-equation turbulence model for aerodynamic flows. In *30th Aerospace Sciences Meeting and Exhibit*, pp. 439.
17. Economou, T.D., Palacios, F., Copeland, S.R., Lukaczyk, T.W. and Alonso, J.J., 2016. SU2: An open-source suite for multiphysics simulation and design. *AIAA Journal*, 54(3), pp.828-846.
18. Williamson, C.H., 1988. The existence of two stages in the transition to three-dimensionality of a cylinder wake.
19. Ma, W., Ottavy, X., Lu, L., Leboeuf, F. and Gao, F., 2011. Experimental investigations of corner stall in a linear compressor cascade. In *ASME 2011 Turbo Expo: Turbine Technical Conference and Exposition*, 54679, pp. 39-51.
20. Kingma, D.P., 2014. Adam: A method for stochastic optimization. *arXiv preprint arXiv:1412.6980*.